Fermi National Accelerator Laboratory

FERMILAB-Pub-88/126-E
[E-741]

Measurement of the Magnetic Field of the CDF Magnet*

C. Newman-Holmes, E. E. Schmidt, and R. Yamada
Fermi National Accelerator Laboratory
P.O. Box 500, Batavia, Illinois 60510

May 1, 1988

*Submitted to Nucl. Instrum. Methods A

MEASUREMENT OF THE MAGNETIC FIELD OF THE CDF MAGNET

C. Newman-Holmes, E. E. Schmidt, and R. Yamada

Fermi National Accelerator Laboratory[1], Batavia, IL

May 1, 1988

Abstract

An automatic field mapping device was constructed at the Fermi National Accelerator Laboratory for the Collider Detector at Fermilab (CDF), and was used to measure the field of the CDF solenoid magnet. The characteristics of the measuring device, the measurement procedure and the data are described.

1. INTRODUCTION

The central part of the CDF detector [1] is structured by a 2000 ton magnet [2] which is excited by a superconducting solenoid [3]. The magnet is composed of an outside return yoke, an end plug at each end and the superconducting solenoid. The central magnetic volume is about 3 meters in diameter and 4.5 meters in length. The magnetic field from this structure was calculated with a computer program [4], but more detailed information may be obtained by measuring the field.

The mapping of this large region requires magnetic field probes which can be moved accurately inside the magnetic field volumes. Therefore, a mechanically stable manipulator is required. To achieve this mechanical stability, carbon fiber channels and honeycomb boards, some made commercially and some made at Fermilab, were developed and used.

In April, 1985, the magnet was excited for field measurement. The magnetic field data from the 1985 measurement have been presented elsewhere [5]. In April, 1986 the magnet was excited with the central calorimeter in place, thus changing the central magnetic field slightly. Also the electromagnetic shower detectors were mounted on the inside surfaces of both end plugs, reducing the measurable volume of the central field at both ends. This paper describes the 1986 measurement.

2. THE FIELD MEASUREMENT DEVICE

The general mechanical features of the mapping device are shown in Figure 1. The major components are the base, the upper and lower carriages, the long cantilevered beam, the rotor, and the shuttle, on which are mounted the sensing elements. The

[1]Operated by Universities Research Association under Contract with the U.S. Department of Energy

whole system is designed so that the sensing elements (search coils) can be placed with a positional accuracy of 0.75 mm in space coordinates and an angular accuracy of $\pm$ 1 mrad.

The sensing elements are moved three-dimensionally in cylindrical coordinates with the origin of the coordinate system at the center of the magnet and the z axis along the solenoid axis. The horizontal axis defines zero for the azimuthal coordinate. On a 9 m long fixed base, a carriage composed of lower and upper parts moves in the z direction. A 6 m long carbon fiber beam is attached to the carriage and a rotor is at the end of the beam. The rotor is rotated azimuthally around the axis of the magnet. A shuttle which carries the probe is moved radially along the rotor. These three-dimensional movements, radial, azimuthal and longitudinal are carried out with stepping motors and a Modulynx controller, manufactured by Superior Electric Co.

The upper carriage may be moved vertically relative to the lower carriage using front and back jacking mechanisms. It may also be moved horizontally using front and back sliding mechanisms. Using these, the z axis of the measuring device is made to be coincident with that of the magnet and the plane of rotation of the rotor is made orthogonal to the z axis within about 1 mrad. The upper carriage may be repositioned relative to the lower carriage to accomodate mapping the far end plug region.

The base was constructed of two steel I-beams and a top plate, welded together with bulkhead plates. It was annealed and stress-relieved. Two parallel 5 cm x 5 cm steel bars were welded on the top plate and their surfaces were machined to a measured flatness of $\pm$ 0.13 mm over their entire length. Attached to the machined surfaces were rails to carry precision linear bearings made by THK Co. in Japan.

The cantilevered 6 m long beam is made of top and bottom carbon fiber U-channels and two carbon fiber honeycomb side plates glued together with six bulkheads made of the same U-channel. The U-channels are 1 cm thick and 15 cm wide, made with prepregnated unidirectional Fortafil 5 manufactured by Great Lakes Carbon. They were pressed and cured by the 3000 ton press which had been used for curing coils for the Fermilab Tevatron superconducting magnets. The side plates are constructed from 1 cm thick honeycomb structure "Floor #7 Type 3" by General Veneer Mfg. Co. The structure is made with Nomex honeycomb and two sheets of carbon fiber plate, each with skin thickness of 0.36 mm.

Inside the beam there are two concentric aluminum tubes. One is used to rotate the rotor and the other to power the shuttle drive along the rotor. They are supported by five sets of three glass bearings, making the tubes straight inside the beam. At the end of the beam there is an aluminum casing which has 15 cm outer diameter copper-beryllium bearings, custom made by Bearing Specialty Mfg. Co.

To reduce the weight and still keep the rigidity of the rotor structure, 2.5 cm thick aluminum honeycomb board was used ("Blue Seal Sandwich Board" made by Hexcel). This material has 0.5 mm thick aluminum skins over an aluminum honeycomb and its surface is quite flat. To reduce eddy current effects in the 1986 measurement, the rotor structure was made completely with carbon fiber using carbon fiber honeycomb boards and custom made carbon fiber solid boards for the guiding rail of the shuttle. The rotor used to map the central solenoid volume was 280 cm long. In addition, a shorter rotor (60 cm) was available for mapping the end plug regions.

The sensing elements are moved along each coordinate (r, z, ϕ) individually. The carriage is moved in the z direction at the speed of 1 cm/sec. The rotor is rotated 360 degrees in 106 sec, corresponding to 8.3 cm/sec at the end of the 280 cm long rotor. The shuttle is moved at the speed of 2.3 cm/sec.

To reduce the effects of eddy currents in the materials, the use of thick aluminum plates near the sensing elements was avoided. Nonmetallic materials were also used as much as possible. When the rotor or shuttle is moved in the fairly uniform central field region, eddy current effects, if any, are small. But when the carriage is moved in regions of nonuniform field, there may be effects from eddy currents in the aluminum shafts or, during the 1985 measurement, in the rotor structure. To reduce the eddy currents in this case, the carriage was moved at the slowest practical speed.

With the manipulator properly aligned, there is about 1 cm clearance between the edge of the rotor and the cryostat wall. To protect the rotor from hitting the magnet, two types of safety interlocks are installed on the ends of the rotor. One is a microswitch with an extended arm. The "Type V3 Miniature Basic Switch V3-129" by MicroSwitch, made of all nonferromagnetic material was used. The other is a proximity switch with a whisker. This switch was custom made at Fermilab.

3. FIELD SENSING ELEMENTS

A search coil system with three components is used to measure the magnetic field in three dimensions. The search coil assembly is identical to that used for the Fermilab ZIPTRACK field mapping device [6]. The output voltages of the search coils are connected to individual integrators and the resultant voltages, which are proportional to the field changes, are sent to an ADC in a CAMAC system. To monitor the drift of the integrators a DVM with a micro-volt range was used.

The sensitivity of the field measurement could be varied by changing the integrator time constants. In the central region, the axial field (B_z) was measured to a precision of 0.5 gauss (less than 0.01% of the operating field of 15 kG). In the end plug regions, B_z was measured with errors on the order of 14 gauss. The radial component of the field

was measured with a sensitivity of 0.5 gauss in the central region and 4 gauss in the end plug regions. The azimuthal component of the field was measured everywhere with a sensitivity of 0.7 gauss.

Ideally the axes of the three component coils should be orthogonal to each other, and the z axis should be parallel to the z axis of the solenoidal magnet. But in reality, there are some errors in their orthogonality and in the alignment of the axes. There is also some imperfection in the radial motion of the rotor and in the transit of the shuttle. These imperfections introduce fictitious radial and azimuthal field components from the huge axial component. If the z axis of the search coil is tilted by α, then the apparent radial or azimuthal components are on the order of αB_z. If B_z is 15,000 gauss and α is 1 mrad, then the error is 15 gauss. To keep the search coil's z axis parallel with that of the magnet, a small survey mirror is mounted on the outside surface of the search coil and is monitored with a transit placed on the z axis outside the magnet.

In the central uniform field region, an NMR probe was used to get precise absolute field values. The NMR probe gave the magnitude of the absolute field to less than 1 gauss. In the central region, the magnitude of the magnetic field is essentially the same as the z component of the field as B_r and B_ϕ are typically less than or on the order of $10^{-3} \times B_z$. During the measurement a second NMR probe was mounted on the inside surface of the west end plug and used to monitor the field at a fixed point for normalization purposes.

4. DATA ACQUISITION AND CONTROL SYSTEM

Data acquisition and manipulator motion control were handled by an IBM-PC interfaced to CAMAC via a Transiac Model 6002 crate controller and a matching expansion board in the IBM-PC chassis. In addition the Modulynx stepping motor controller was commanded by the PC through a CAMAC GPIB interface module. The IBM-PC was used only for primary data acquisition and system control. Raw data were transferred via an RS-232 serial link to a Digital Equipment VAX for further analysis and also for online graphical display of measurement data.

Motions of the shuttle, rotor, and carriage were accomplished by individual SLO-SYN stepping motors through the Modulynx controller. One high power Modulynx motor driver was needed for the large carriage stepping motor while two smaller Modulynx drivers were used for the shuttle and rotor.

The alignment axes (front and back jacks and front and rear slides) used to align the upper carriage were powered by four separate SLO-SYN stepping motors. These motors were controlled by the combination of Joerger SMC-24P CAMAC stepping motor controllers and drivers originally designed and built at Fermilab.

Except during movement, the axes drives were locked in placed by electrically actuated brakes. The individual brake interfaces were controlled through bits in a CAMAC output register. The system contained a number of motion limit switches interlocked to the brakes and motor driver power supplies. The status of these bits could be queried through the PC via a CAMAC input register.

Positions of the various axes were read by a variety of different encoders. The carriage and rotor were monitored with BEI Electronics, Inc. absolute rotary encoders. The outputs of the absolute encoders were directly read into CAMAC input registers as binary values. The radial position of the shuttle was marked at a series of fixed points by an arrangement of a microswitch on the shuttle and a precision notched rail. The output of the microswitch was monitored through both a CAMAC up/down counter and an input register. All axes including the alignment axes were also monitored by incremental encoders pulsing into CAMAC up/down counters (Kinetic Systems model 3640).

The output of the search coil integrators and a magnet current transductor were fed into a multi-channel "simultaneous sample and hold" ADC, LeCroy CAMAC Model 8212A/32. The BCD outputs from the two NMR probes were put into Joerger quad input register CAMAC modules. Figure 2 shows a block diagram of the data acquisition system.

The main controlling program was written in IBM BASIC. To obtain sufficient operating speed, the BASIC program was compiled and linked to an assembly language CAMAC driver supplied by Transiac. The driver was modified to more conveniently support compiled BASIC and 24 bit CAMAC data transfers. A single call to CAMAC took about 0.3 msec. The software and IBM-PC operated very reliably with virtually no down time for either system, software, or hardware failure.

Much of the software was devoted to setup and system checkout. Constants and calibrations were read from a data file to eliminate the need for program recompilation for minor system changes. Run dependent parameters were stored and recalled for the operator so that only changed parameters needed to be entered. All CAMAC modules were checked for response in the initialization phase of the software. After initialization and setup, the software was driven by operator keyboard commands. The main data command allowed the operator to specify for one of the principal axes a start point, stop point, and probe sampling interval. Most data were taken by sweeping the rotor through 360 degrees, taking data every 10 degrees. The carriage would then be moved to a new z position and another sweep of the rotor taken. Since the primary probes (search coils) measured only relative field changes, data sweeps with the carriage (z) and the shuttle (r) were also needed to tie all the data points together along with normalization values from the NMR probes.

At the end of each data sweep, the data were sent to the VAX and immediately examined for possible anomalies. Two operators usually ran the system; one to control data taking and one to examine the data. A map of 2000 points on the surface of a 2.4 m diameter by 3.8 m long cylinder took about eight hours and generated about 160 kbytes of character data.

5. GENERAL FEATURES OF THE FIELD MEASUREMENT

For most of the measurements, the magnet was operated at its nominal current of 5000 amps, corresponding to a field of 15 kilogauss. The axial field component is directed toward negative z. Most of the field measurement was done with the three dimensional search coils and with a stationary NMR as a standard. But the field distribution near the center of the magnet was scanned in detail with an NMR probe. Nonuniformities in the field due to joints in the conductor and to the solenoid return lead were studied extensively. The residual field, present when the magnet is turned off, was also measured.

For complete field mapping, the field was measured on the boundary of a cylindrical surface and these data were then used to perform a fit based on Maxwell's equations. The fit coefficients were used to calculate values of the magnetic field inside the cylinder. These calculated values were then compared to measurements of the field within the cylindrical surface.

5.1 Field Distribution on the Magnet Axis

The field distribution along the axis of the magnet was measured using search coils and an NMR probe. Figure 3 shows the axial component of the field on the magnet axis, as measured by a search coil. The positions of the inner and outer surfaces of the end plugs are indicated with arrows. The outer surfaces of the end plugs are at $z = \pm 372$ cm and the inner surfaces are at $z = \pm 226.5$ cm. The central uniform region was measured in detail with an NMR probe; the results are shown in Figure 4. The peak of the field is about 20 cm from the geometrical center. Several factors may contribute to this shift, including a nonuniform distribution of the conductor joints, nonuniform windings of the conductor over the length of the solenoid, or a slight displacement of the solenoid relative to the center of the iron structure.

5.2. Residual Magnetic Field Distribution

The field distribution was measured with a Hall probe when the excitation current was zero. Figure 5 shows the axial component B_z measured at r = 26 cm. Measurements of the residual field taken with search coils indicate that the residual field on the magnet axis (r = 0) is essentially the same as that at r = 26 cm. The positions of the inner and

outer surfaces of the end plugs are again indicated with arrows. The axial component has its maximum value at points roughly 40 cm inside the surfaces of the end plugs. The residual field has a local minimum value at the magnet center where it is about 5 gauss. Inside the end plug regions, the axial component of the residual field reverses polarity. The residual fields are due to the saturation of the iron so the field is strongly localized near the inside edges of the end plugs.

5.3. Effect of Conductor Joints

The CDF solenoid has 1174 turns wound on a single layer. The conductor of the superconducting solenoid has ten joints distributed along its length. The average distance between the joints is about 50 cm. Two full turns are welded together to make each joint effectively decreasing the number of turns to 1164.

The measured data near the conductor are shown in Figure 6. The positions of the innermost six joints are shown with arrows. These data were taken at r = 135 cm; the conductor is at r = 149 cm. There are several clear dips in B_z corresponding to the joints. B_r also shows variations correlated with the positions of the joints. From a computer calculation, one finds that the expected value of the decrease in B_z is about 60 gauss at a radial distance of 14 cm from a joint [4]. This is in good agreement with the observed values.

5.4. Effect of Return Lead

The solenoid has a return conductor at r = 152.7 cm just outside the solenoid winding at the top of the coil. The return lead runs parallel to the axis of the solenoid near $\phi = 90°$. With the approximation that the return current is infinitely long, and neglecting the effect of nearby steel, the field due to the return lead may be estimated with a simple equation:

$$B_{ret.lead} = I/(5R) \tag{1}$$

where R is the distance from the return conductor. Here B is in gauss, I is in amperes and R is in cm. The observed effect is shown in Figure 7. The azimuthal component of the magnetic field B_ϕ was measured with a search coil at r = 135 cm at several z positions throughout the magnet. B_ϕ shows a strong peak near $\phi = 90°$, where the return conductor is placed. A fit to the observed data indicates that the return lead is at $\phi = 83°$. The peak is between 55 and 60 gauss, in good agreement with the value expected from the equation above (56.5 gauss).

5.5. Field Distribution in End Plug Regions

The field distribution in the east end plug region is shown in Figure 8. The B_z and B_r components are plotted for r = 5, 15 and 25 cm at $\phi = 0°$. The positions of both surfaces of the end plug are indicated in Figure 8 with arrows. The data for the west end plug are similar. These distributions agree well with computer calculations.

6. FITTING THE MAGNETIC FIELD

There are two advantages to fitting the magnetic field. First, it allows a check for the consistency and validity of the data. Second, it is neither practical nor necessary to measure the magnetic field at every point inside the solenoid. Once one has some assurance that the fit is reliable, it may be used to calculate the magnetic field at any point in the solenoid. The fitting of the magnetic field data was performed using a procedure due to H. Wind [7]. In a region free of sources, the magnetic field obeys Maxwell's equations in the form:

$$\nabla \cdot B = 0 \qquad and \qquad \nabla \times B = 0 \tag{2}$$

Then one may write the magnetic field as the gradient of a potential function ψ with :

$$B = \nabla\psi \qquad and \qquad \nabla^2\psi = 0. \tag{3}$$

A general solution to Laplace's equation in cylindrical coordinates may be written in the form:

$$\begin{aligned} \psi(r,z,\phi) &= \sum_{m,k} C_{mk} \left\{ \begin{array}{c} sin(m\phi) \\ cos(m\phi) \end{array} \right\} \left\{ \begin{array}{c} sinh(kz) \\ cosh(kz) \end{array} \right\} J_m(kr) \\ &+ \sum_{m,k} D_{mk} \left\{ \begin{array}{c} sin(m\phi) \\ cos(m\phi) \end{array} \right\} \left\{ \begin{array}{c} sin(kz) \\ cos(kz) \end{array} \right\} I_m(kr) \end{aligned} \tag{4}$$

where the first part of the solution corresponds to the case where the potential is zero on the cylindrical surface but nonzero on the cylinder end plates and the second part of the solution is for the case of zero potential on the cylinder end plates with a nonzero value for the potential on the cylindrical surface.

By differentiating equation (4), one can write down an expression for the magnetic field. Then the procedure is to use observations of the field on the cylinder surface to fit for the coefficients C_{mk} and D_{mk}. Once these coefficents are determined, the magnetic field may be calculated at any point inside the cylinder.

One limitation of this fitting method should be noted. If one uses only observations of B_z to fit for the coefficients, the resulting solution will be incomplete. Any currents in the z direction will give rise to magnetic fields transverse to z but with no component

component along z. The fitting procedure is thus "blind" to any fields arising from currents in the z direction. The CDF solenoid has a return lead with current flowing in the z direction; effects of this return lead on the radial and azimuthal components of the magnetic field will not be included in the calculation based on the fit. Properly, one should use observations of the magnetic field everywhere normal to the cylinder surface to determine the field inside. Practically speaking though, the z component of the field is much easier to measure as inside a solenoid, the field is very nearly in the z direction. So for this analysis, observations of B_z were used to fit the magnetic field. But the field due to the solenoid return lead was added to the solution from the fitting program before comparison with the measurements of B_r and B_ϕ.

Data were taken on several cylindrical surfaces. Each cylindrical surface consists of a "mantle" at constant r and two "endplates" each at constant z. For the largest cylinder mapped in the central region, the mantle was at r = 135 cm with measurements made every 10° in ϕ and every 10 cm in z. The endplates were at z = −130 cm and z = 150 cm with measurements made every 10° in ϕ and every 15 cm in r. Additional measurements were made within each cylindrical volume to check the results of the fit. In the central region, B_z was measured with a sensitivity of 0.5 gauss

The coefficients were determined using a program from the CERN Computer Centre Program Library [8,9]. This program has been used by the CLEO collaboration at the Cornell Electron Storage Ring to fit the magnetic field of their solenoid [10]. Because of a limitation of the program (the number of zeroes of the Bessel functions used by the program was limited) only ϕ measurements taken every 30° were used by the fitting program. The remaining measurements were used to check the results of the fitting program. A total of 240 coefficients were found in the central region. This number was increased to 528 with no noticeable change in the results.

The program was used to fit the magnetic field in the central region. Figure 9 shows measurements of the axial component of the magnetic field (B_z) compared to calculated values based on the magnetic field fit at r = 0 and 135 cm. Here the points shown are the measured values and the values calculated from the fit are represented by solid lines. The agreement is excellent. Figure 10 shows a histogram of the difference between the measured and calculated values of B_z for the central region. The mean is 0.02 gauss with an RMS of 0.47 gauss. This is in good agreement with the σ expected (1 ADC count was 0.5 gauss as mentioned above). Less than 20% of the points entered into Figure 10 were actually used to determine the fit coefficients. The conclusion is that the program does a very good job fitting the z component of the magnetic field in the central region.

We next examine the radial (B_r) component of the field. Figure 11a shows his-

tograms for the difference between the measured and calculated values of B_r. This histogram has an RMS value considerably higher than that of the B_z histogram. We note that because the axial component of the field is so much larger than the transverse components, small misalignments of the field mapping apparatus can lead to spurious measurements of the r and ϕ components of the magnetic field. An investigation was performed to determine whether such misalignments could account for the observed data. As the azimuthal component of the magnetic field is quite small throughout the central region (< 65 gauss, with an average value of 10 gauss), the alignment study was limited to the radial component of the field.

The misalignment study uses three parameters. Two of them (denoted α and ϕ_0) specify the axis of the rotor with respect to the z direction; α is the angle between the z axis and the rotor axis. In addition, the search coil assembly may contain some small misalignments so that all three coils are not exactly mutually perpendicular. Let the third parameter, denoted β, be defined as (90° – the angle between the z axis and the axis of the r search coil). Then α and β will be small if the apparatus is aligned properly. If a measurement is performed with the rotor turning about its axis, then added to any genuine radial component of the magnetic field, there will be a shift of magnitude βB_z and an oscillation in ϕ with amplitude αB_z. The procedure is then to fit the observed data plus terms due to misalignment to the calculated values of B_r. If one does the fit for the misalignment parameters over various subsets of the data, a consistent picture emerges for the parameters. One finds for α the value 1.52 ± 0.07 milliradian. The values for β and ϕ_0 are consistent with 0.

Figure 11b shows a histogram of the difference between B_r (calculated) and B_r (measured and corrected for misalignment). The mean is -0.97 gauss compared to 6.4 gauss for the uncorrected data. The RMS decreases from 17 gauss to 4 gauss.

7. CONCLUSION

A new device to map large magnetic field volumes has been built using novel lightweight nonmagnetic materials. This device has been used to map the magnetic field of the CDF solenoid. A long cantilevered support beam eliminates the need for supporting structures at the ends of the volume to be mapped. A set of field measurements on a cylindrical boundary surface was successfully used to calculate the magnetic field at other points on the surface and within the boundary.

Acknowledgements

We thank operators from the Fermilab Magnet Test Facility and External Beam Line for their help with data taking. We especially express our thanks to J. Hawtree, R. Leverence, and J. Schallenberger for the construction and operation of the field mapping device. We want to acknowledge Mr. M. Noguchi of Tsukuba University who contributed to this project in its early stage of preparation. We also thank Dr. A. Tollestrup of Fermilab and Prof. A. Melissinos of Rochester University for stimulating discussions.

References

1. Design Report for the Fermilab Collider Detector Facility, Fermilab Internal Report, CDF Note No. 111, August, 1981.

2. J. Grimson et al., "Magnetic Structure of CDF Central Detector", in Proceedings of the 12th International Conference on High-Energy Accelerators, Fermi National Accelerator Laboratory, Batavia, Illinois, August, 1983 (p. 639).

3. Design Report for an Indirectly Cooled 3-m Diameter Superconducting Solenoid for the Fermilab Collider Detector Facility, Fermilab TM-1135, October, 1982; H. Minemura et al., "Construction and Testing of a 3 m Diameter x 5 m Superconducting Solenoid for the Fermilab Collider Detector Facility (CDF)", NIM in Physics Research A238, 18 (1985); R.W. Fast, et al., "Testing of the Superconducting Solenoid for the Fermilab Collider Detector", Fermilab TM-1334, July, 1985.

4. R. Yamada, "Magnetic Field Calculation on CDF Detector (I)", Fermilab TM-1162 and CDF Note No. 150, January 20, 1983.

5. R. Yamada, et al. "The CDF Field Mapping Device - ROTOTRACK", Fermilab TM-1358 and CDF Note No. 345, August, 1985; R. Yamada, C. Newman-Holmes and E. E. Schmidt, "Measurement of the Magnetic Field of the CDF Magnet", Fermilab TM-1369 and CDF Note No. 346, November, 1985; C. Newman-Holmes, "Fitting the Magnetic Field of the CDF Solenoid", CDF Note No. 361, November, 1985.

6. R. Yamada, et al., Nucl. Inst. and Meth. 138, 567 (1979).

7. H. Wind, IEEE TRANSACTIONS Magnetics 5, 269 (1969); H. Wind, Nuclear Instruments and Methods 84, 117 (1970);

8. Paul R. Ganci, "Fitting a Magnetic Field from Boundary Observations in Cylindrical Coordinates", CERN Computer Centre Program Library Long Writeup W1029/W1030.

9. You Hua Hu, "The 'Wind-Model' of a Magnetic Field in Cylindrical Coordinates", CERN Computer Centre Program Library Long Writeup W1043.

10. P. Ganci and A. C. Melissinos, "The Field Map of the CLEO Magnet (Warm Coil)", CBX-80-53, September, 1980.

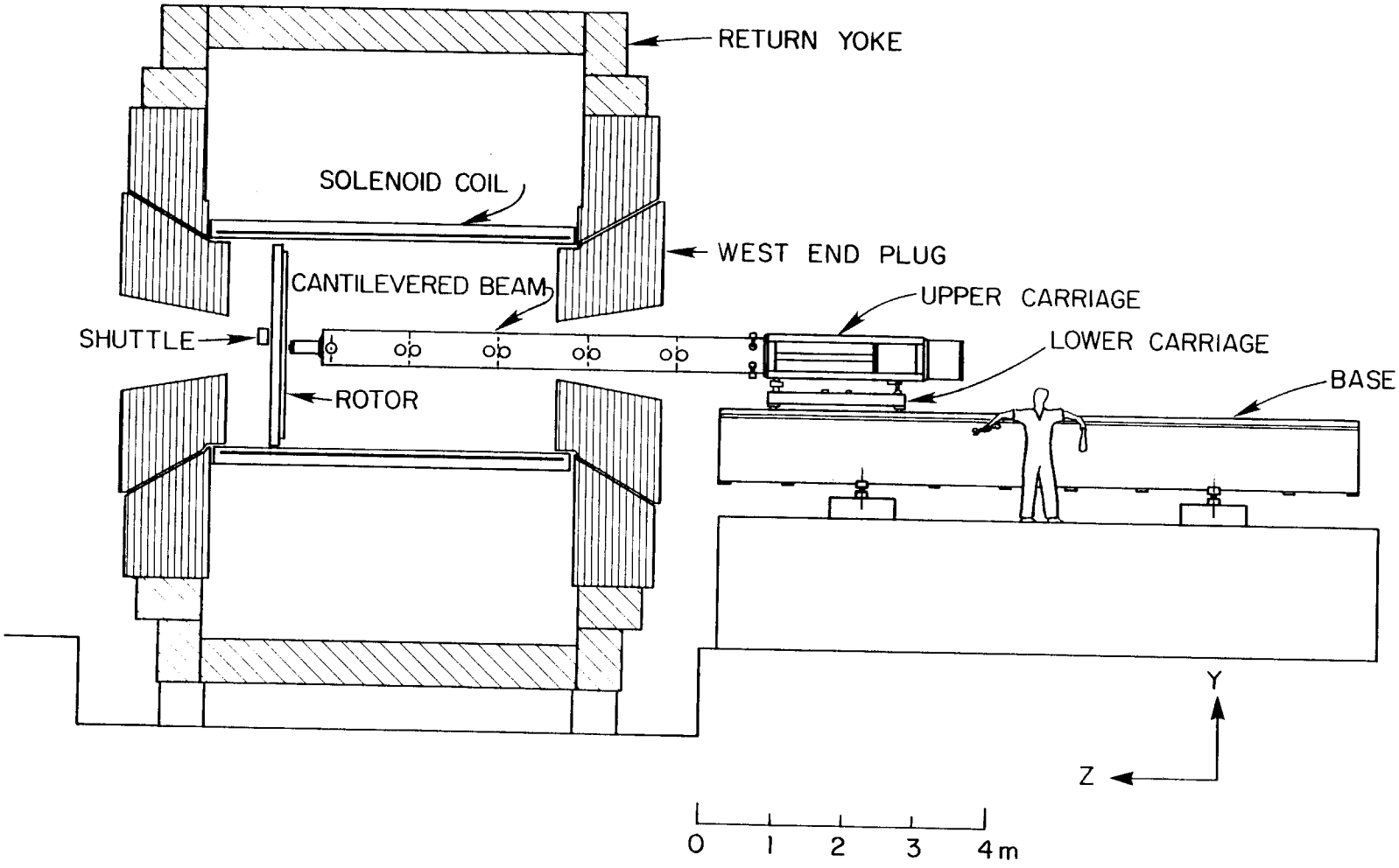

CDF FIELD MAPPING DEVICE

Fig. 1 The CDF field mapping device.

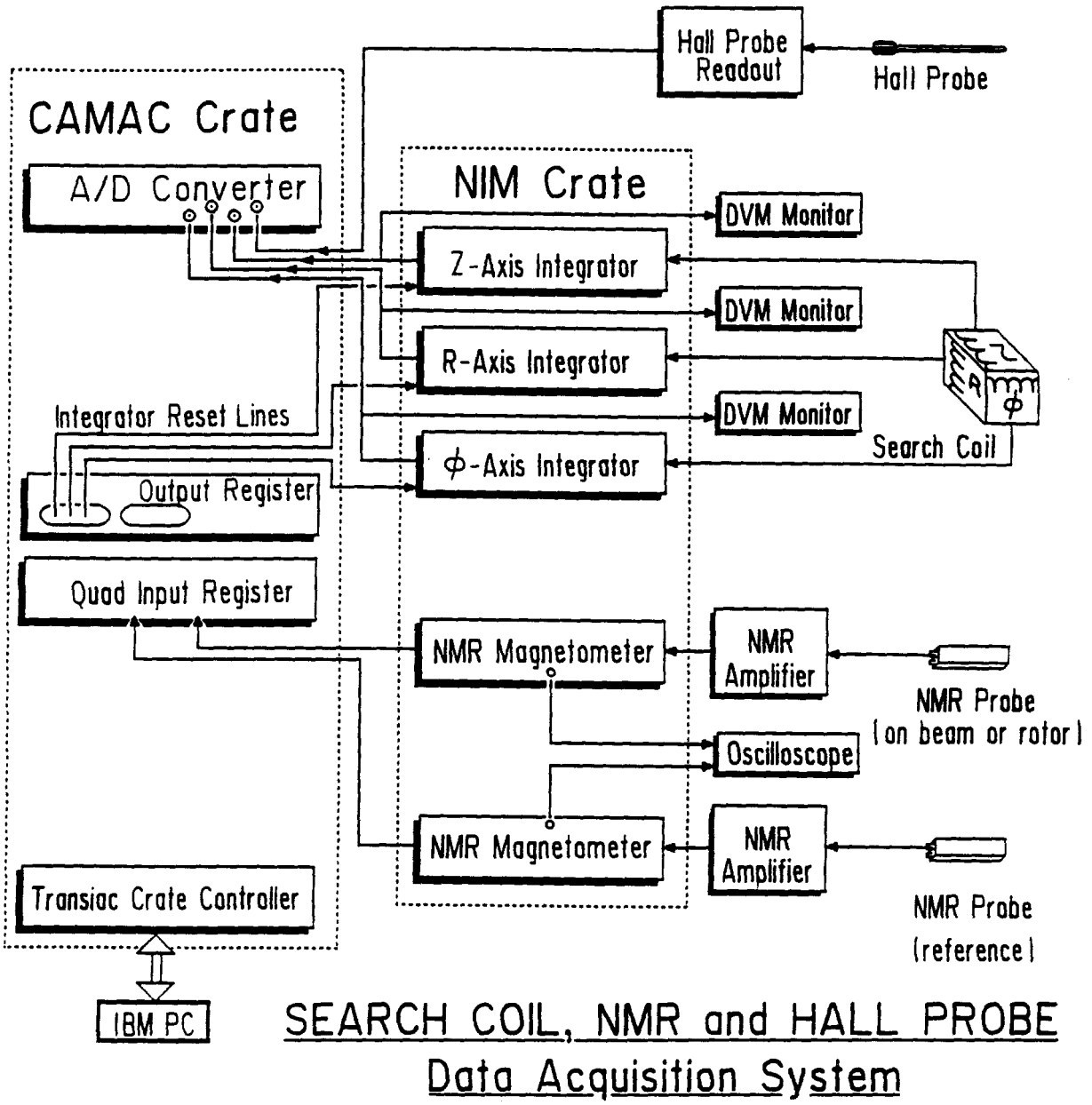

Fig. 2 Block diagram of the data acquisition system.

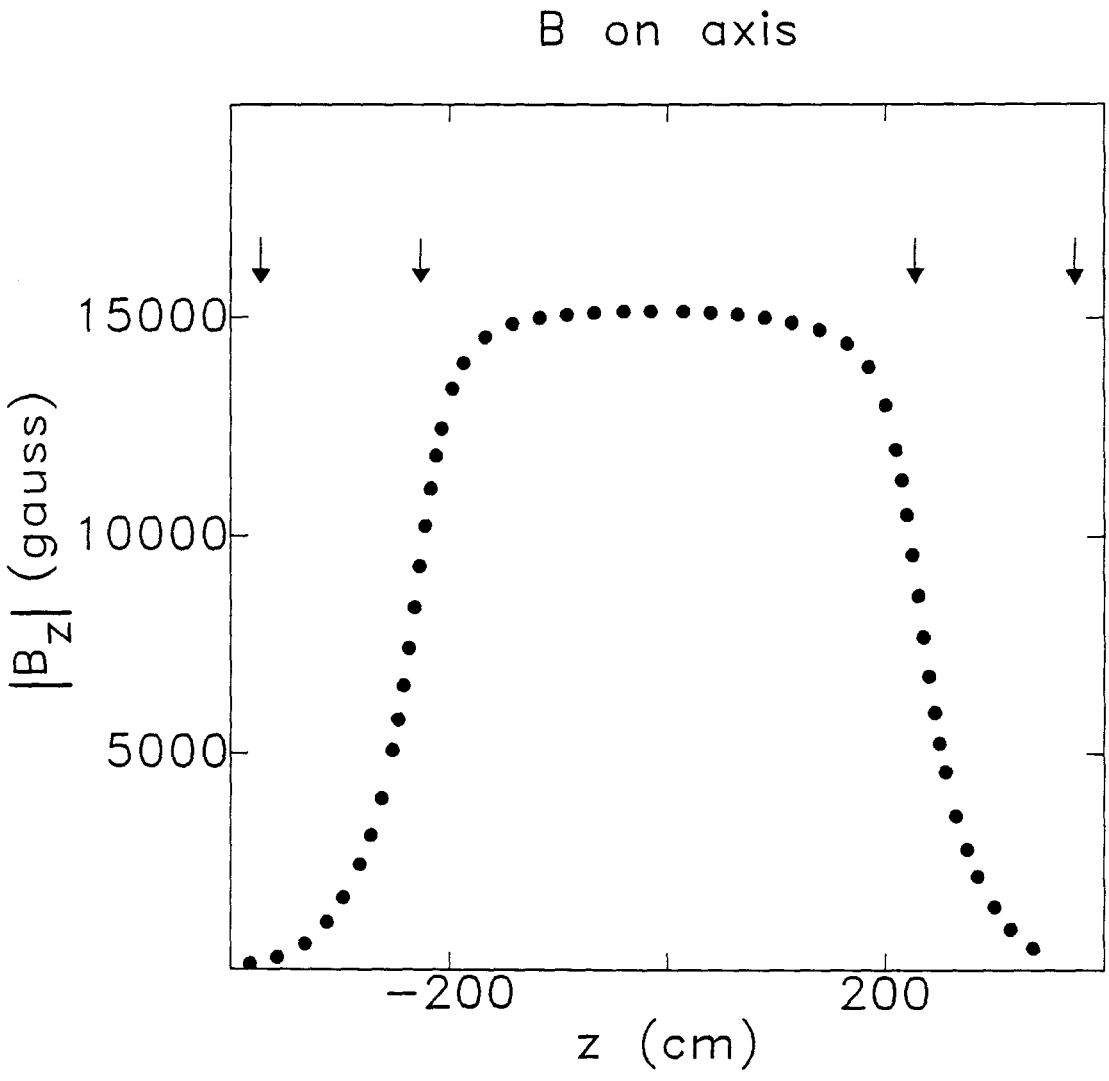

Fig. 3 Magnitude of B_z on the axis of the solenoid.

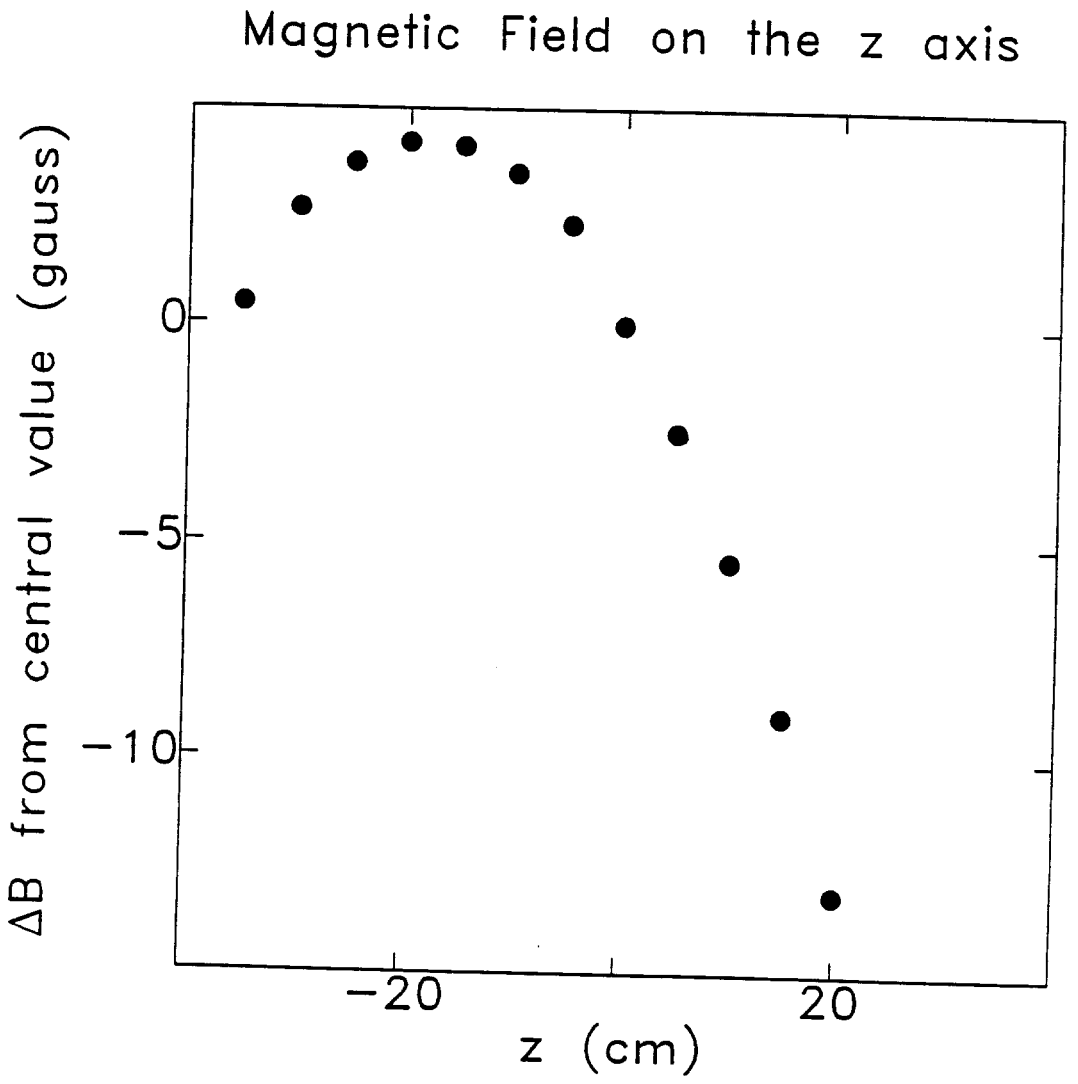

Fig. 4 Detailed magnetic field distribution on the z axis in the central region as measured with NMR.

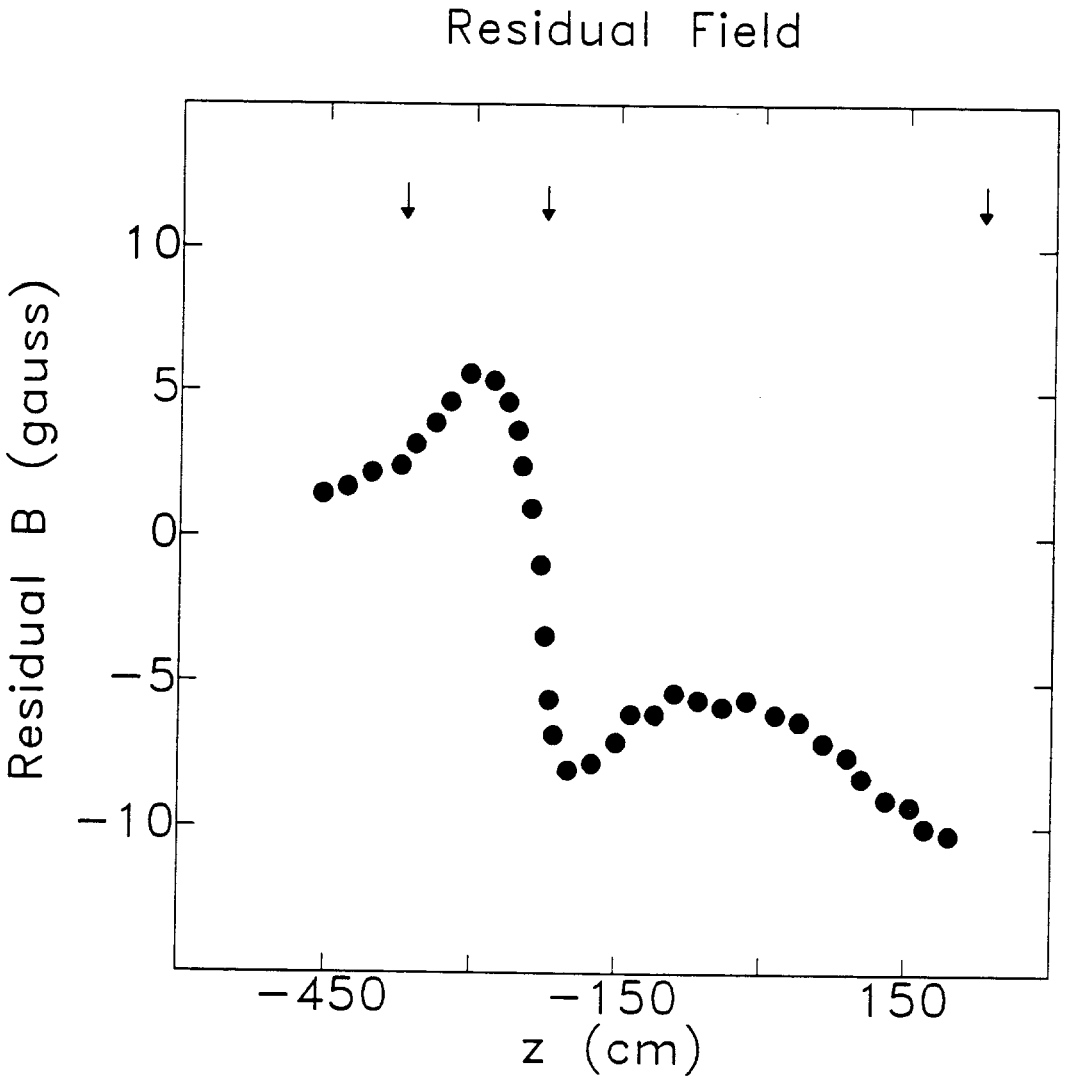

Fig. 5 The axial component of the residual field.

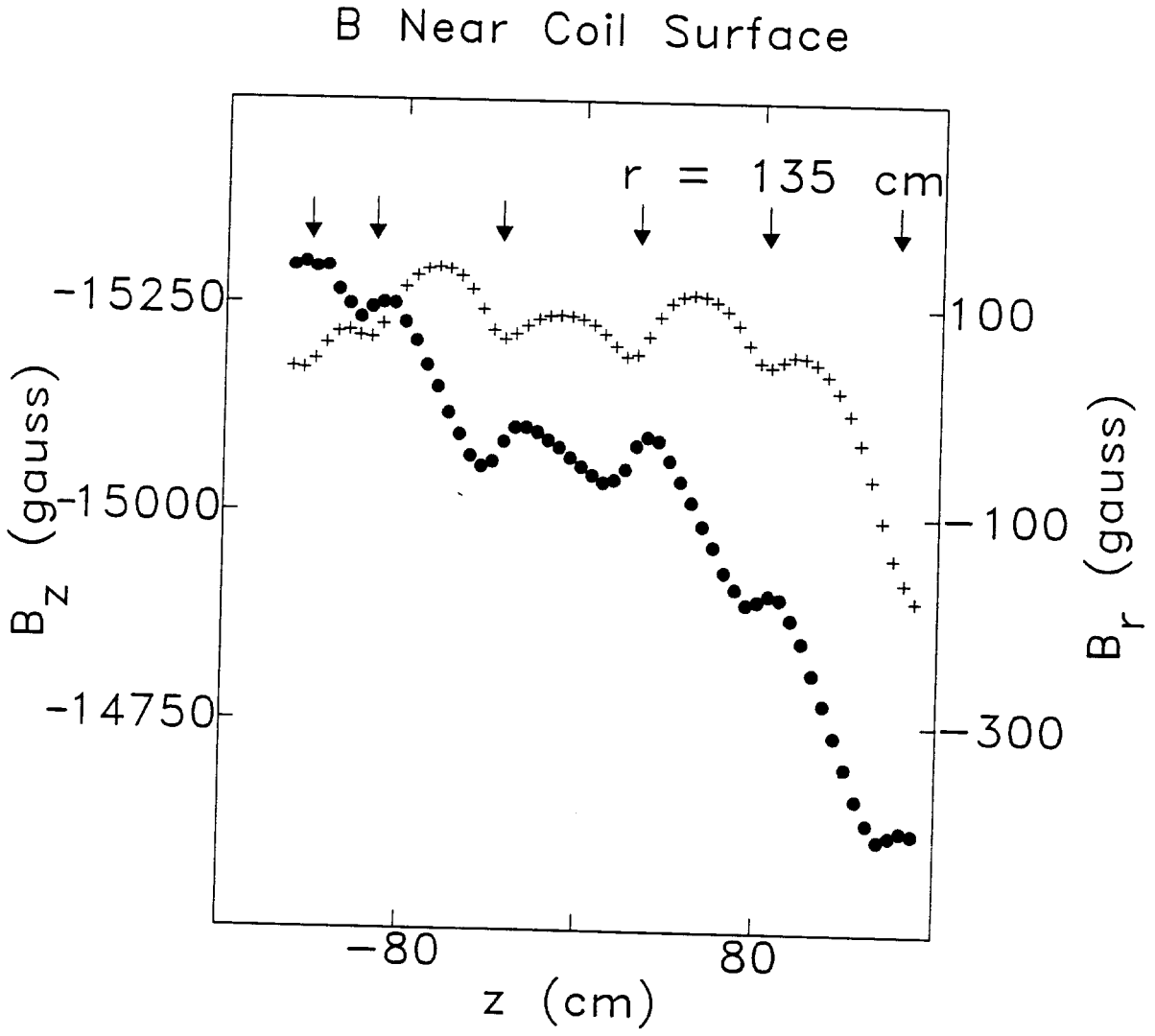

Fig. 6 B_z and B_r near the solenoid surface, showing the effects of joints in the conductor. The dots show the radial component of the field and the crosses show the axial component. Note that the axial component of the field is in the -z direction.

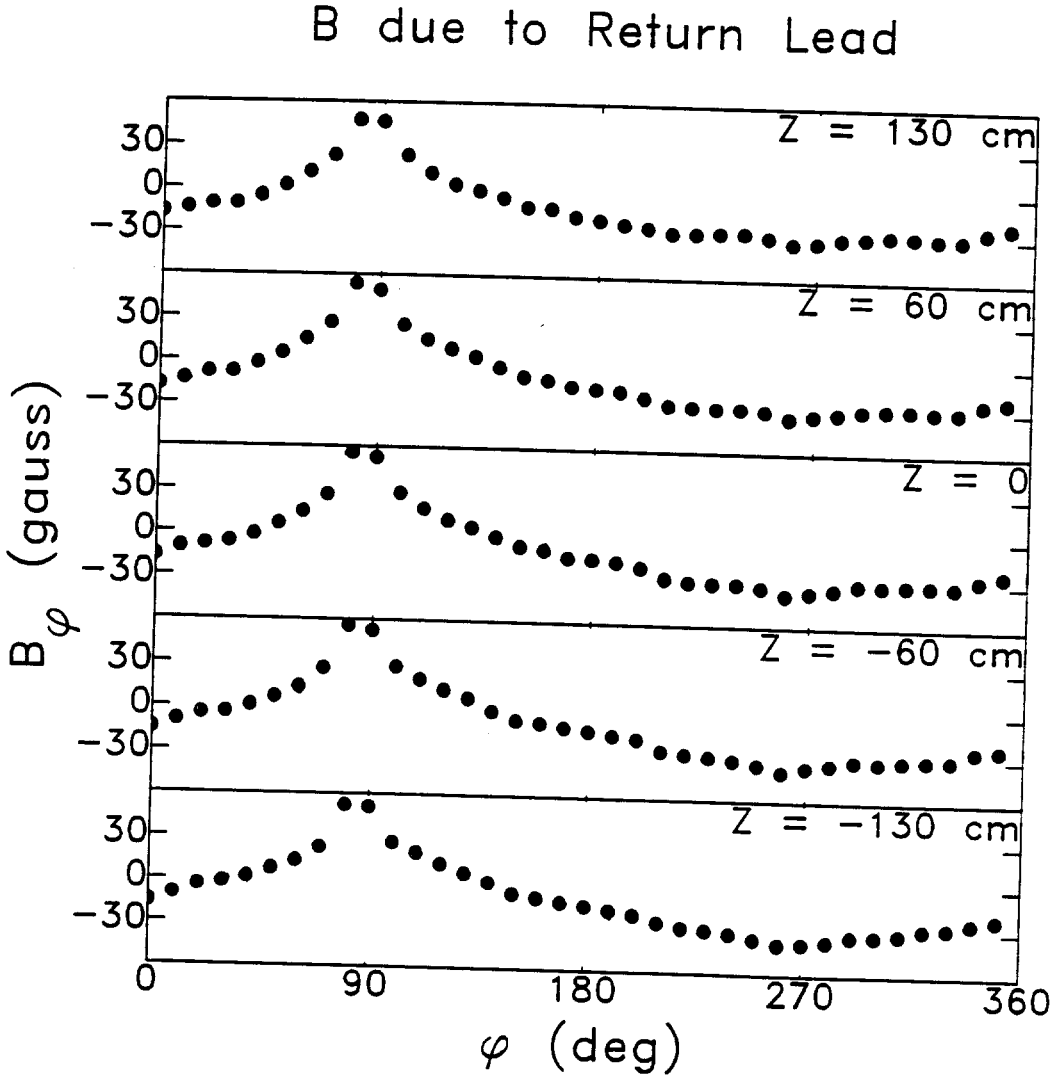

Fig. 7 Azimuthal component of the magnetic field near the solenoid surface, showing the effect of the return bus at $\phi = 83^{\circ}$.

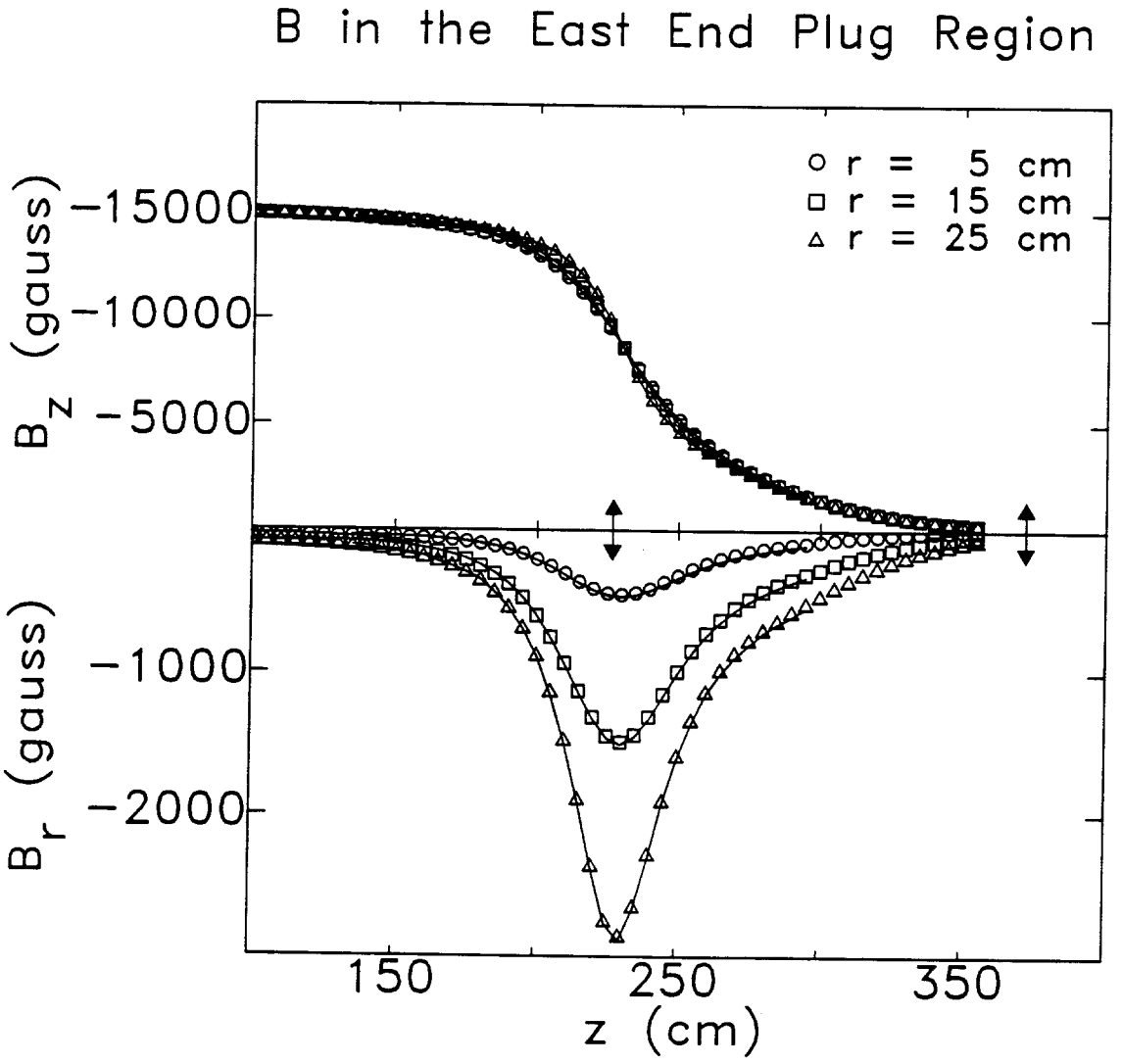

Fig. 8 B_z and B_r in the east end plug region.

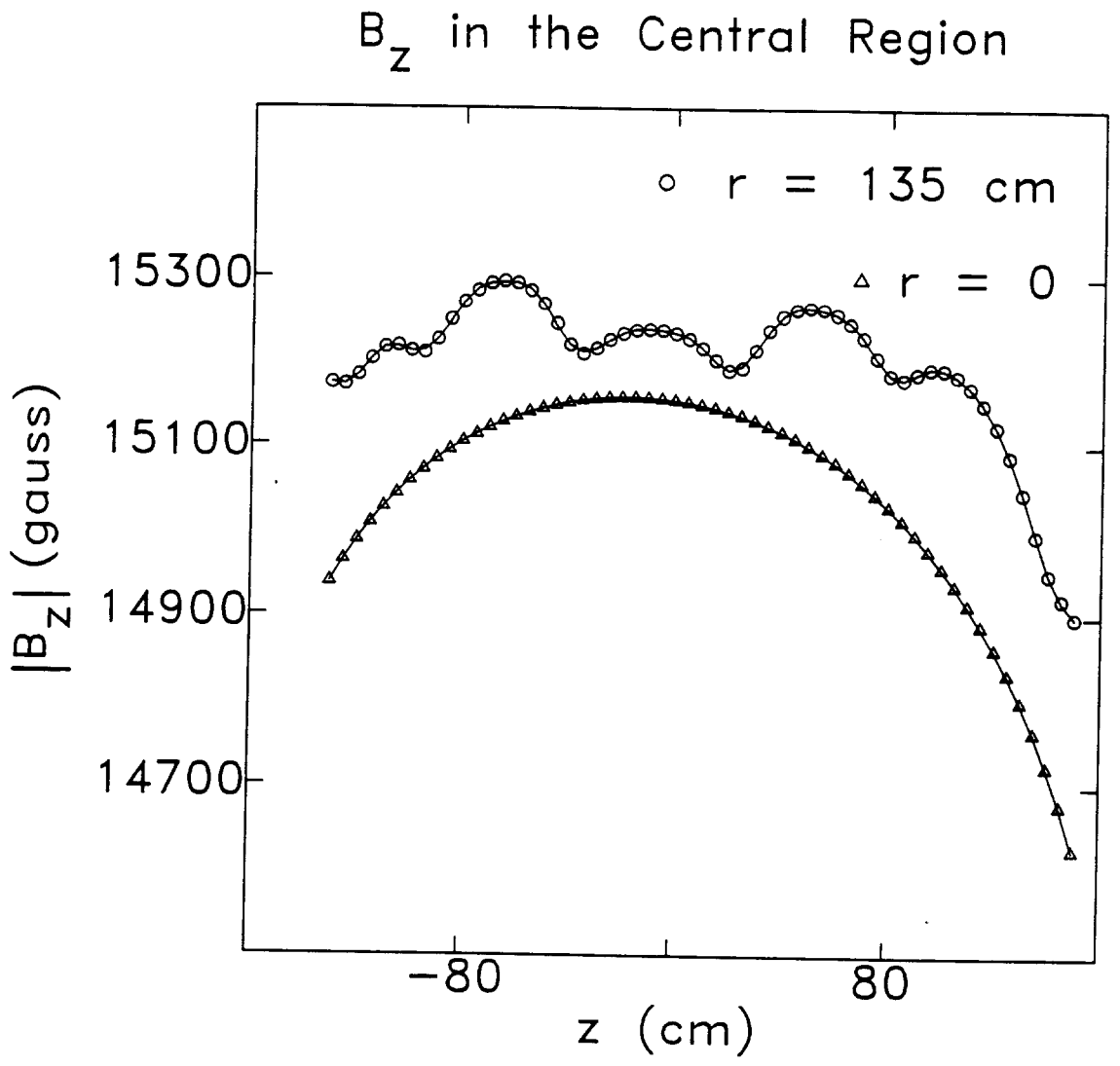

Fig. 9 Magnitude of B_z at r = 0 and r = 135 cm along the magnet.

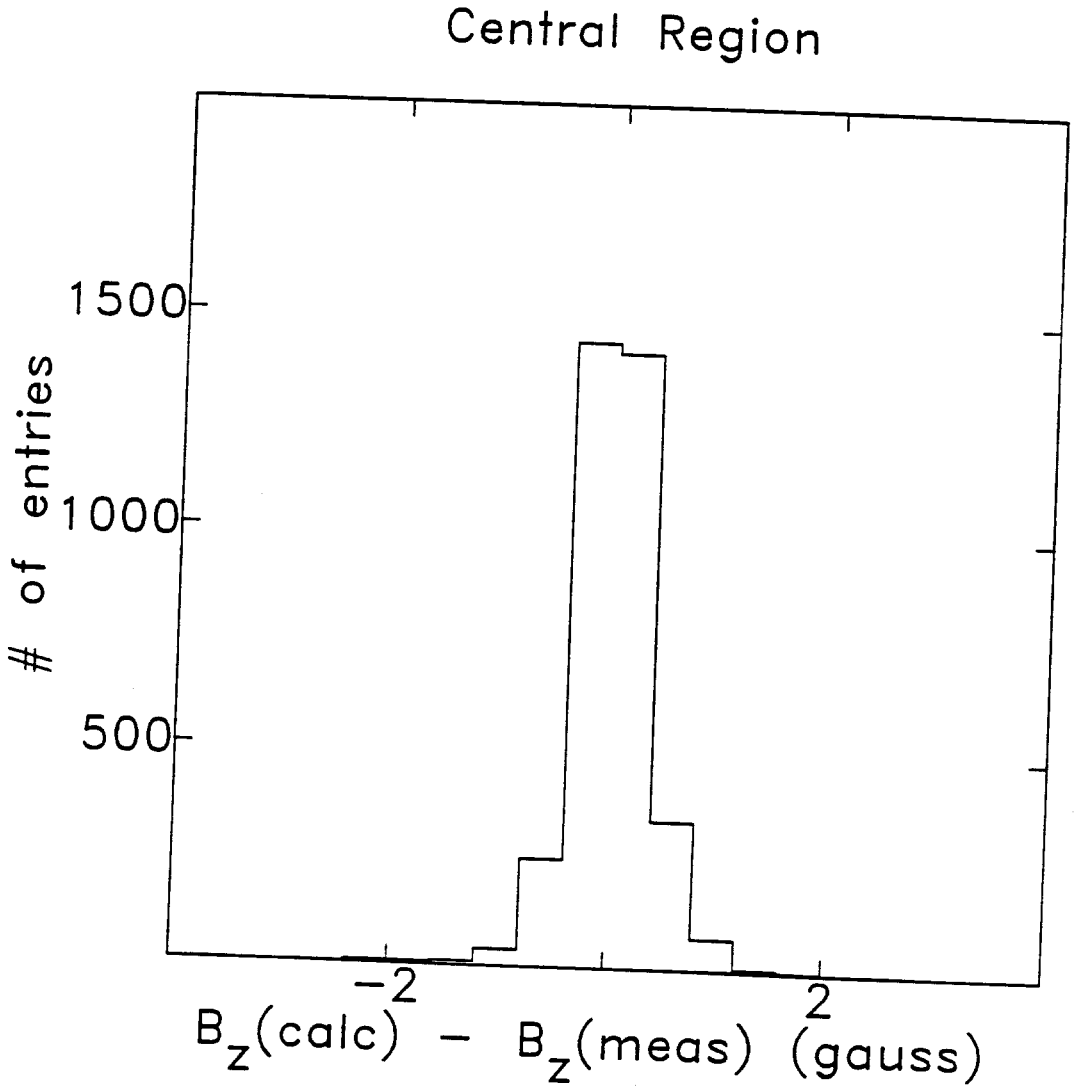

Fig. 10 Distribution of B_z(calc) - B_z(meas) for the central region.

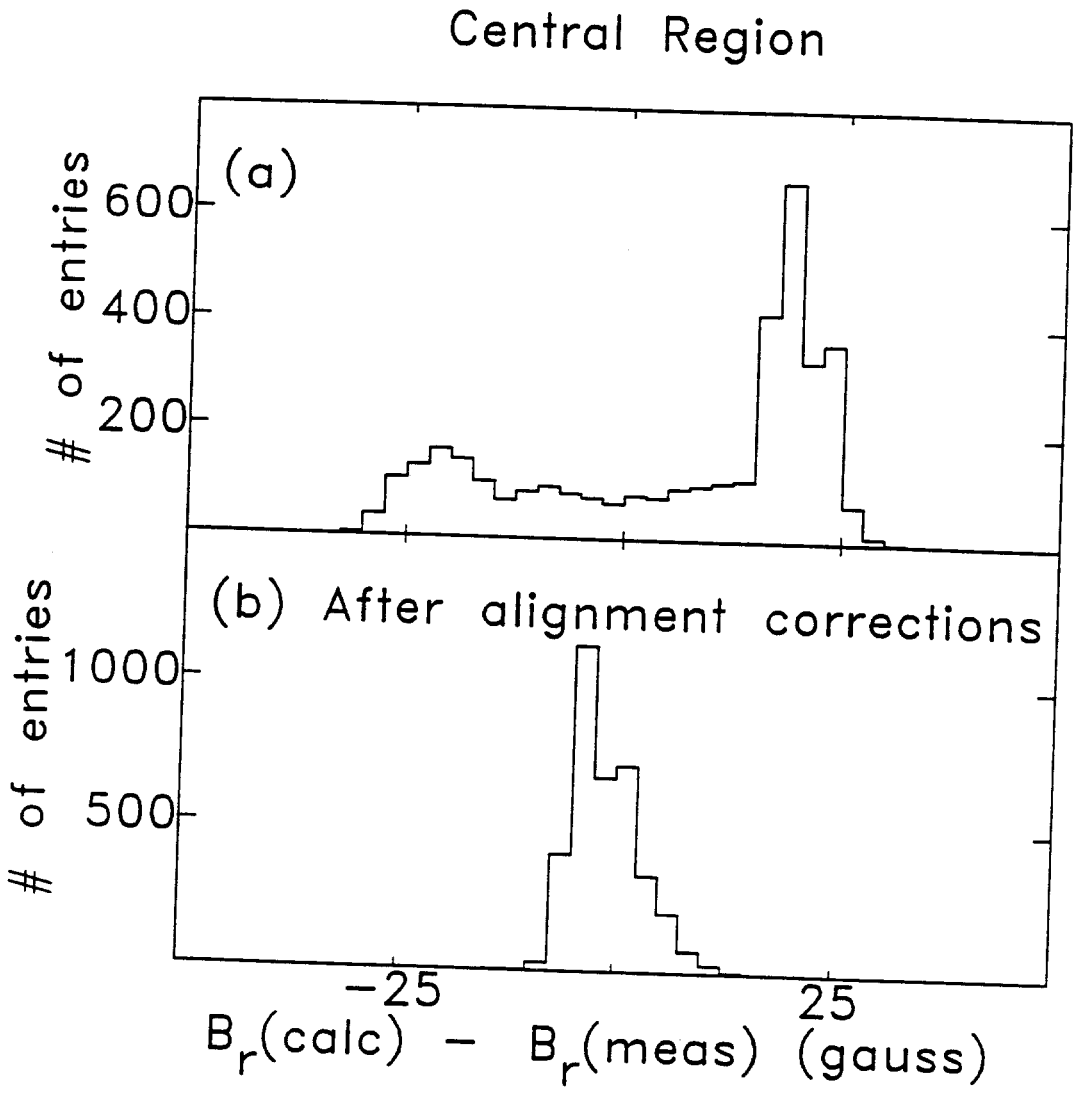

Fig. 11 (a) Distributions of B_r(calc) - B_r(meas) for the central region and (b) Distribution of B_r(calc) - B_r(meas) in the central region after alignment corrections described in the text.